

Sea surface temperature estimation from the Geostationary Operational Environmental Satellite 12 (GOES 12)

C J Merchant¹, A R Harris², E Maturi², O Embury¹, S N MacCallum¹, J Mittaz² and C P Old¹

¹School of GeoSciences, University of Edinburgh, Edinburgh, Scotland

²NOAA/NESDIS/ORAD/ORAD, Camp Springs, Maryland

Corresponding author: C J Merchant, Crew Building, King's Buildings, Edinburgh EH9 3JN, UK;
chris@staffmail.ed.ac.uk

Abstract

This paper describes the techniques used to obtain sea surface temperature (SST) retrievals from the Geostationary Operational Environmental Satellite 12 (GOES-12) at the National Oceanic and Atmospheric Administration's Office of Satellite Data Processing and Distribution. Previous SST retrieval techniques relying on channels at 11 and 12 μm are not applicable, because GOES-12 lacks the latter channel. Cloud detection is performed using a Bayesian method exploiting fast forward modelling of prior clear-sky radiances using numerical weather predictions. The basic retrieval algorithm used at night-time is based on a linear combination of brightness temperatures at 3.9 and 11 μm . In comparison with traditional split window SSTs (using 11 and 12 μm channels), simulations show that this combination has maximum scatter when observing drier colder scenes, with a comparable overall performance. For day-time retrieval, the same algorithm is applied after estimating and removing the contribution to brightness temperature in the 3.9 μm channel from solar irradiance. The correction is based on radiative transfer simulations, and comprises a parameterisation for atmospheric scattering and a calculation of ocean surface reflected radiance. Potential use of the 13 μm channel for SST is shown in a simulation study: in conjunction with the 3.9 μm channel it can reduce the retrieval error by 30%. Some validation results are shown, while a companion paper shows a detailed analysis of the validation results for the operational algorithms described in this present article.

1 Introduction

The National Oceanic and Atmospheric Administration's Office of Satellite Data Processing and Distribution have been generating operational sea surface temperature (SST) retrievals from the Geostationary Operational Environmental Satellites (GOES) since December 2000. There are two platforms: GOES-E, situated at longitude 75° W, and GOES-W at 135° W. Geostationary orbit allows the acquisition of high-temporal-resolution SST retrievals. The geostationary sensor provides thermal IR radiance data of sufficient precision to permit retrieval of sea surface temperature (SST) with accuracy approaching that of polar-orbiting sensors. The GOES-SST products generated from these algorithms include hourly regional sectors, 3-hourly hemispheric imagery, and 24 hour merged composites.

Since 2000, GOES-SST has become the most requested NOAA satellite product for the U.S. coastal user community. The datasets have been invaluable for a wide range of environmental studies, including coastal and open ocean, fisheries, climate, numerical weather prediction and ocean and high seas forecasting. The accurate GOES-SST data allows the climate community users to account for the diurnal SST effects.

GOES-12 became the operational GOES-E platform on April 1, 2003, replacing the ageing GOES-8. The latter was the original 3-axis GOES platform launched in 1994. The GOES 8/9/10 imager, with three infrared channels (3.9, 11, and 12 μm), required a significant investment of resources over several years to generate SST products approaching AVHRR-like quality. Since the GOES-12 satellite imager has only two channels (3.9 and 11 μm) available to generate SSTs, this heritage could not be directly transferred. The 3.9 μm channel is difficult to use during the day because of solar contributions to the signal that derive from surface reflection and atmospheric scattering. The GOES-12 algorithm required a substantial departure from current operational methodology to ensure continued availability of daytime GOES-SST retrievals. Continuity of operations required the generation of GOES-12 SSTs for the numerous users of these products. This paper describes the GOES-12 SST algorithms developed for operational implementation from April 1, 2003, including subsequent improvements to the processing. Centers other than NOAA have generated GOES-SST products operationally (May and Osterman, 1998; Brisson et al., 2002), but to our knowledge no others are attempting to derive day-time SST products for GOES-12 in the absence of the 12 μm channel.

2 GOES-12 Imager

The main difference for the purpose of this paper between the GOES-12 Imager and previous instruments in the series is that it is the first to have a channel at 13.3 μm . The spectral response of this channel falls in the wing of the strong CO_2 absorption band centered at 15 μm and the channel is therefore primarily sensitive to temperatures in the lower troposphere. This additional information is used to improve the height assignment of cloud-track winds (especially for sub-pixel and semi-transparent clouds) via the CO_2 -slicing approach. However, this new channel has replaced the one centered at 12 μm . The 12 μm channel is a key component of the SST retrieval algorithm applied to data from previous GOES Imagers, which used the 3.9, 11 and 12 μm channels at night and, critically, is dependent on just the 11 and 12 μm channels for the daytime product. Given the success of the GOES-SST product, it is highly desirable to establish a new scheme for continuing its production using the revised Imager specification, especially since a 12 μm channel will not be available until GOES-R, which is currently scheduled for launch in 2012.

Figure 1 shows the normalized spectral response functions of GOES-12 channels at “3.9”, “11” and “13” μm (together with those for a typical polar-orbiter channel set, in this case the Along Track Scanning Radiometer-2 at “3.7”, “11” and “12” μm) with the atmospheric transmittance for mid-latitude conditions. The sensitivity of GOES-12’s 13 μm channel to surface temperature is small, given the low channel-integrated nadir transmittance of, typically, 0.3 (range ~ 0.05 to 0.5).

3 Night-time SST retrieval

a. Cloud detection

The first step in retrieval of sea surface temperature using infrared imagery is the detection of image pixels whose radiances are significantly affected by the present of cloud in their field of view. The approach to cloud screening adopted for GOES-12 operations is an implementation of the probabilistic, physically based method of Merchant et al. (2005). The reader is referred to Merchant et al. (2005) for a description of this method (and a brief review of alternative methods), and is referred to the algorithm theoretical basis document for the details of the implementation for GOES-12 (available from NOAA/NESDIS/ORAD). The cloud-screening method is only very briefly described in the remainder of this sub-section.

The GOES-12 cloud detection is based on forward modeling of the expected observations and their error covariance, followed by application of a formulation of Bayes’ theorem to generate an estimate of the probability that each pixel is cloud-free given the actual observations. The approach is thus explicitly formulated to match the underlying nature of the cloud-detection problem. Cloud detection is always an attempt to assess the likelihood of an observation being cloud-free given both the observation itself and prior information about the nature of both cloud-free and cloudy observations. Often the prior information is embedded, perhaps somewhat obscurely, in the thresholds of the various cloud screening tests applied. In our “Bayesian” approach, the prior information being used is made explicit, which makes the approach general and maintainable. Moreover, we benefit from being able to derive this prior information from forecast fields available within an operational center for numerical weather prediction.

Numerical weather prediction (NWP) forecast fields (surface temperature and wind speed, and temperature and water vapor profiles) are used as input to the Community Radiative Transfer Model (CRTM) to predict the clear-sky brightness temperatures at 3.9 and 11 μm and their error covariance for each pixel in the image. This error covariance includes the effect of sampling error from the mis-match in scale between the prior surface temperature field (on the model grid) and the pixel-resolution observations. The predicted brightness temperatures and their error covariance define a joint Gaussian

clear-sky brightness temperature probability distribution for the observations (see Merchant et al., 2005, Eq. 6).

The night-time observation vector used for cloud detection also includes the local standard deviation (LSD) of both brightness temperatures across a 3-by-3 box centered on each pixel; the “forward model” for the LSD is a combination of the contribution to clear-sky LSD expected from radiometric noise (uncorrelated between channels) and the contribution from any frontal SST gradient in the vicinity of the pixel. The presence of a front of strength dT_s/dx (where T_s is SST and x is distance perpendicular to the front) can be shown to cause an LSD in a 3-by-3 box of pixels with ground resolution l of approximately

$$\sqrt{\frac{3}{4}} \frac{dT_s}{dx} l \frac{\partial T_\lambda}{\partial T_s} \quad (1)$$

independent of the orientation of the front relative to the image pixels. T_λ is the channel brightness temperature, with the channel wavelength λ being either 3.9 μm or 11 μm . The LSD from such a front is correlated between the channels. At present, the probability of a front being present and the strength of any such front are set to global constants. The obvious refinement of updating these parameters in the light of recent high-resolution SST analyses is yet to be explored and implemented, and one of the difficulties faced is that frontal features in high resolution SST products are not in general consistently reproduced and are subject to artifacts from some analysis procedures (e.g., www.mersea.eu.org/Satellite/sst_validation_14_glob_oi.html). Figure 2 shows an example of the joint LSD distribution obtained for GOES-12 by the above means.

The probability density functions describing the distribution of brightness temperatures and LSDs of cloudy pixels are also required. At present, globally fixed distributions are used, which are shown in Figure 3. These have been derived from cloud-flagged observations of 3.7 μm and 11 μm brightness temperature in 1 km resolution images of the second along-track scanning radiometer (ATSR-2), aggregated up to 5 km boxes and with added synthetic radiometric noise, to be more representative of the GOES-12 imager resolution and noise levels. The variability in cloudy brightness temperatures is large compared to the differences in brightness temperatures arising from the different spectral responses of ATSR-2 to GOES-12 (Figure 1), so that using the ATSR-2-based probability density function for GOES-12 screening performs adequately well. GOES-12 specific probability density functions based on radiative transfer modeling are under development and test at time of writing.

We have described above how we define probability density functions for brightness temperatures and local standard deviation. Together with the actual brightness temperatures and local standard deviation, Bayes’ theorem states how to estimate the probability of the location being clear-sky. The output of the cloud detection step is therefore a probability of being clear-sky for each pixel. A single threshold can now be defined to create a cloud-mask, namely the threshold of probability of clear below which we mask the pixel (i.e., do not calculate an SST). If the priority is for the SST estimates made to be accurate, we can be conservative and set this threshold at a high level (close to 1.0). If the priority is avoiding major cloud contamination while maximizing the area for which reasonable SST estimates can be formed, we can be lax and set the threshold relatively low (e.g., at 0.5). At present, we use a threshold of 0.8 (i.e. SST is not calculated for pixels below this probability). The most accurate SST retrievals are expected to be obtained for probabilities closest to 1.0, and the probability is retained as part of the SST product to satisfy users with different accuracy/coverage requirements. The Bayesian probability is also used, therefore, to define a “proximity confidence value” that ranks SSTs obtained into five quality categories, consistent with the framework of the Global Ocean Data Assimilation Experiment High Resolution SST Pilot Project (Donlon et al., 2007). For details of the interaction of this threshold and statistics on the validation of GOES-12 SST, see the companion paper by Harris et al. (2007, manuscript submitted to *J. Atmos. Oceanic Technol.*).

b. Sea surface temperature estimation

The main novelty of the GOES-12 imager from the viewpoint of SST estimation is the replacement of one of the traditional “split-window” channels (that at 12 μm) with a 13.3 μm channel (see section 2). The operational night-time SST retrieval therefore uses only the 3.9 μm and 11 μm channels.

Linear split-window estimators rely on the approximate proportionality of the atmospheric effect on brightness temperatures between channels at 11 μm and 12 μm . The main absorbing gas for split window channels is water vapor, and the proportionality between the channels is least strict at high water vapor loadings when the atmospheric transmittance in the 12 μm channel approaches zero. Split-window estimators of SST therefore tend to be noisiest at high atmospheric water vapor loadings. Because of the latitudinal correlation of SST and atmospheric water vapor, it is broadly the case that split window SSTs tend to be noisiest where SSTs are warmest. Furthermore, the dependence of the proportionality between $T_s - T_{11}$ and $T_s - T_{12}$ on water vapour means that linear split-window estimators have bias trends that are also generally related to scene temperature.

SST retrieval estimators using the 3.9 and 11 μm channels have a somewhat different characteristic, as shown in Figure 4: the greatest scatter tends to be at lower SSTs. Figure 4 is based on the radiative transfer simulations undertaken for defining GOES-12 retrieval coefficients for SST. NWP data from all seasons and times of day were sampled at the locations shown in Figure 5 and were used as inputs to the MODTRAN4 radiative transfer model run at 1 cm^{-1} spectral resolution in order to calculate brightness temperatures for GOES-12 channels at the appropriate satellite zenith angle. The formulation of the SST estimator is

$$\hat{T}_s = a_1 + a_2 F_\theta + (a_3 + a_4 F_\theta) T_{3.9} + (a_5 + a_6 F_\theta) T_{11} \quad (2)$$

where $F_\theta = \sec(\theta) - 1$, θ is the satellite zenith angle, and the a_i are the “retrieval coefficients” found by linear regression. Their values are: $a_1 = -2.09$, $a_2 = 1.15$, $a_3 = 1.177$, $a_4 = 0.073$, $a_5 = -0.162$, and $a_6 = -0.069$. Errors in the characterisation of sensor spectral response can lead to the retrieval coefficients based on radiative transfer being sub-optimal. As discussed in Merchant and Le Borgne (2004), such errors seem in practice principally to affect the bias of the retrievals such that the offset coefficient, a_1 , requires adjustment in the light of validation data. Figure 4 was then created by applying the retrieval coefficients back to a similar but independent set of simulated brightness temperatures with added noise representative of GOES-12. The overall simulated retrieval error in Figure 4 is 0.36 K. The increased scatter at lower SSTs arises as follows. The heaviest weight among the retrieval coefficients is on $T_{3.9}$ because it is the channel for which transmittance is higher and less variable (less sensitivity to water vapor). Variability in $T_s - T_{3.9}$ is more strongly influenced by the temperature of the atmosphere than $T_s - T_{11}$, because dry-air absorption (mainly from CO_2) is more significant, particularly when water vapor loadings are low. $T_s - T_{11}$ can therefore correct only part of the variability in $T_s - T_{3.9}$. In the tropical regions of high SST, the atmospheric and surface temperatures are tightly coupled, with air-sea temperature differences varying relatively little. In middle and high latitudes, the coupling of atmospheric and surface temperatures is less tight, with a wider range of air-sea temperature difference, stronger near surface inversions, and more variable lapse rate. Therefore, the uncorrectable variability in $T_s - T_{3.9}$ tends to be greater in the middle and high latitudes where the surface temperature is low.

In the GOES-12 products, associated with each SST retrieval is a (pseudo-) random retrieval error estimate which varies from pixel to pixel. This error estimate is formulated as:

$$\varepsilon_{SST} = \sqrt{(w_{3.9} \varepsilon_{3.9})^2 + (w_{11} \varepsilon_{11})^2 + (\varepsilon_{RET})^2} \quad (3)$$

where $w_{3.9} = a_3 + a_4 [\sec(\theta) - 1]$, $w_{11} = a_5 + a_6 [\sec(\theta) - 1]$ -- i.e., are obtained from the retrieval equation (2). The assumed noise-equivalent differential temperatures (NEdT) in the two channels are $\epsilon_{3.9} = 0.15$ K and $\epsilon_{11} = 0.20$ K. (An obvious refinement is to make these NEdT depend on brightness temperature, since the same radiometric noise is equivalent to a larger NEdT at colder temperatures, because of non-linearity in the Planck function, especially at 3.9 μm .) ϵ_{RET} is an estimate of the intrinsic retrieval error associated with the formulation of the SST estimator. At present a single global value is assumed, derived from the global standard deviation of the scatter evident in the retrieval simulations shown in Figure 4; the evident dependence of the standard deviation on SST is not parameterized in ϵ_{RET} at present. The other comment to make about ϵ_{RET} is that it is representing errors that are not wholly random. Day-to-day changes in surface and atmospheric state do cause associated errors in retrieved SST that appear random, but which have non-zero mean in a longer term average. In other words, there are systematic errors that contribute to the retrieval error, which Merchant et al (2006) have identified as “prior” and “non-linearity” error; the most significant characteristic for SST estimation of these forms of error is that they contribute bias that varies geographically and seasonally. The prior error is associated with the climatological difference between the state and the average state implicit in the regression data from which coefficients are derived (whether these data are based on radiative transfer modeling or empirical matches). The non-linearity error is the inability of any linear or simple non-linear SST estimator to capture the non-linearity in the relationships between state and observations. Merchant et al. (2006) identified that these forms of bias can be estimated by detailed forward modeling. It has been common practice to ignore the mix of random and systematic error when discussing SST validation studies and in making SST retrieval error estimates. The approach described above for pixel-by-pixel error estimation within the GOES-12 operations is a step toward refining the products supplied operationally to reflect the known variable characteristics of SST error, with a view to improving the service provided particularly to sophisticated users such as centers for data assimilation.

See the companion paper by Harris et al. (2007, manuscript submitted to *J. Atmos. Oceanic Technol.*) for an assessment of the performance of the current operational GOES-12 SST, and the influence of air-sea temperature difference on retrieval errors.

4 Day-time SST retrieval

a. Solar contamination in the 3.9 μm channel

Estimating SST from day-time imagery of GOES-12 is challenging compared to doing so from night-time imagery and compared to doing so from the day-time imagery of earlier GOES imagers with a 12 μm channel. This is because, in the absence of a 12 μm channel, the channel at 3.9 μm has to be used, despite the fact it contains potentially significant contributions to its radiance from scattered and reflected solar irradiance. (Use of the 11 and 13 μm channels together for SST retrieval was explored by radiative transfer simulation, giving a simulated SST retrieval error of 1.7 K, which is not a useful precision. Retrieval of SST with 11 and 12 μm relies on the fact that these two channels are differentially sensitive to essentially the same atmospheric parameters. This is not true of the combination of 11 and 13 μm .)

We deal with the solar contamination of the 3.9 μm channel by attempting to estimate and remove the solar contribution to radiance before undertaking cloud screening and SST estimation: we create a “pseudo-nighttime” $T_{3.9}$ image. As will be shown below, there is limited precision to which the solar contamination can be corrected. Quantitative correction, cloud screening and retrieval are therefore only undertaken away from the main area of sun glint.

The pseudo-nighttime $T_{3.9}$ is formed by correcting for the effects of atmospheric scattering and sun glint. These corrections also have error estimates associated with them that are propagated into the cloud screening and SST retrieval in addition to the estimated radiometric noise.

The radiance in the 3.9 μm channel is estimated using a parameterization based on the following considerations: (i) the number of scattering particles in the atmosphere viewed by the satellite is proportional to the path length at the satellite zenith angle, i.e., to $\sec(\theta)$; (ii) the transmittance of the solar irradiance in passing through the atmosphere from Sun-to-surface-satellite is $\tau^{(\sec\theta+\sec\vartheta)}$, where τ is the global mean nadir transmittance and θ is the solar zenith angle. We fitted the parameters, b_i , in an equation for the path-scattered solar radiance observed by the sensor, L_{scat} :

$$L_{scat} = (b_1 \sec \theta) b_2^{(\sec \theta + \sec \vartheta)} + b_3 \quad (4)$$

This solar radiance was simulated by MODTRAN4, assuming marine-type aerosols, and using a surface meteorological visibility of 10 km, 23 km and 50 km. The locations of simulation were as before, each location being run with the Sun at a several elevations above the horizon. The performance of the parameterization in simulation is illustrated in Figure 6a, for the case of a surface meteorological visibility of 23 km. Despite its simplicity, the parameterization captures a significant proportion of the variance (40%) in the 3.9 μm brightness temperature difference associated with solar radiance scattered in the atmosphere into the GOES-12 line of sight. The error in the estimate of the change in brightness temperature is 0.37 K. For the smaller changes, up to 1.5 K, the error is 0.25 K, capturing 47% of the variance.

Given a prior estimate of surface meteorological visibility, the coefficients for the three pre-calculated visibilities can be interpolated with respect to the reciprocal of the prior visibility. However, the operational code at present assumes a fixed the visibility of 27 km. As is evident from Figure 6b, there is a significant dependence on the visibility that could be addressed by using an operational prior. More generally, this parameterization does not account for any azimuthal dependence of scattering, and doesn't use prior information about atmospheric transmittance; it is therefore somewhat limited, and is in fact a temporary expedient. Once a fast radiative transfer model is available operationally that includes scattered solar radiance at 3.9 μm , the parameterization will be superseded.

In addition, it is necessary to estimate the solar radiance reflected by the surface of the ocean into the sensor's view. This is calculated as

$$L_{refl} = \left[\frac{\rho(\omega) \sec^4(\theta_n) P(z_x, z_y)}{4 \cos(\theta)} \right] \times \Omega_{SUN} \times L_{SUN} \times \tau \quad (5)$$

where: $\rho(\omega)$ is the water reflectivity, which depends on the angle of incidence ω to glinting facets of the water surface; θ_n is the facet normal at the point of reflection; $P(z_x, z_y)$ is the probability of facets oriented with θ_n given the upwind (z_x) and crosswind (z_y) slopes of the glinting facets; Ω_{SUN} is the solid angle subtended by the sun; L_{SUN} is the solar radiance integrated over the 3.9 μm channel, 230.6 $\text{W m}^{-2} \text{str}^{-1}$; and τ here is the two-way transmittance of the atmosphere. We derive the water reflectivity from Hale and Querry (1973), and the facet slope probability density function is that of Cox and Munk (1954), which is parameterized in terms of 12.5 m wind speed.

The radiances with the L_{refl} contribution subtracted are converted to brightness temperature changes using the channel-integrated radiance-to-brightness-temperature relationship, the difference between these and the radiance not so adjusted being ΔT_{GLINT} . The sun-glint effect on SST is then calculated as

$$\Delta T_s = [a_3 + a_4 (\sec(\theta) - 1.0)] \times \Delta T_{GLINT} \quad (6)$$

and a "valid" pseudo-nighttime $T_{3.9}$ is only estimated if this evaluates to less than 1.0 K, since the error in ΔT_{GLINT} is estimated as 20% and stronger glint will degrade the SST retrieval significantly. Figure 7 illustrates the magnitude and extent of ΔT_{GLINT} (by showing the spatial distribution of $T_{3.9} - T_{11}$, which is dominated by the effect of solar contamination in the glint region) and examples of the 1 K contour outside of which a valid pseudo-nighttime $T_{3.9}$ is considered valid.

b. Day-time cloud screening

The day-time cloud screening is based on an observation vector comprising the visible reflectance (channel 1 of the imager), the 11 μm brightness temperature, the LSD of the visible reflectance, and the LSD of the 11 μm brightness temperature. At present, a simple analytic parameterization of the visible reflectance of the ocean under clear sky is used as the forward model for channel 1. This involves parameterizing the overall ocean albedo in terms of solar zenith angle, and then applying an anisotropy function (e.g., Kidder & Vonder Haar, 1995) to the albedo to estimate the observed reflectance; the anisotropy function is a function of satellite and solar zenith angles, and of their relative azimuth angle. Given that atmospheric variability and ocean roughness are not considered, the estimated error is 50%, which is sufficient given the typically large ratio between clear-sky and cloudy-sky reflectance, and allows for normal variations in marine aerosols. We assume a uniform frequency distribution of cloudy-sky reflectance. The distribution of the local standard deviation of the clear-sky visible reflectance is based on estimated instrumental noise alone: i.e., it is assumed that real reflectance variations over length scales of 3 pixels are negligible for clear-sky ocean. The distribution of the LSD of the cloudy-sky visible reflectance is assumed to be uniform between 0% and a maximum value; this maximum value is calculated for a hypothetical extreme situation where 3 pixels within the 3-by-3 box have 100% reflectance and the remainder have 0% reflectance; given that is a maximum reflectance contrast and that the assumption of complete filling or non-filling of pixels is extreme, this provides a sensible maximum for LSD. The above set of assumptions and approximations are sufficiently effective to be employed in this first-generation algorithm, but are not the optimum representation. Because the Bayesian approach decomposes the problem of cloud detection into specifying these distributions, the way in which we will obtain further improvements in cloud detection is clear: we will increase the realism of the distributions for visible reflectance and its local standard deviation.

c. Sea surface temperature estimation

The same retrieval equation (2) is used for day-time SST estimation as for night-time, but with the pseudo-nighttime $T_{3.9}$ replacing the actual 3.9 μm brightness temperature. For the SST retrieval error estimate, the NEdT for the 3.9 μm channel is augmented by an independent error in the solar-radiance correction, estimated to be 20% of the correction at nadir and rising to 100% of the correction at a satellite zenith angle of 80° (i.e., typically less than 0.5 K, but up to a few kelvin in unfavorable configurations).

5 Ongoing developments

a. Cloud detection

The operational cloud detection code for GOES SST operations was the first implementation of the Bayesian screening approach outlined by Merchant et al. (2005). An ongoing project (Mackie et al., 2008) is developing a modular, generic implementation of cloud detection software based on this approach, which will become the operational GOES SST cloud detection in the near future. This software library will also be generally and freely available under a public license. Within that framework, the future development of the cloud detection algorithms will involve two improvements. Firstly, when the functionality of the CRTM is expanded to cover fast forward modeling of the GOES visible-channel transmittance, we will replace the albedo-based forward model for visible reflectance with the CRTM and the surface reflectance model based (as with the glint correction estimate) on forecast winds. Secondly, and more tentatively, we will assess the use of the 13 μm brightness temperature available with GOES-12 for Bayesian cloud detection. The 13 μm channel is designed to assist height determination of cloud tops, and thus includes cloud information in its signal; but in terms of mere cloud detection (as opposed to cloud parameter retrieval), the added information it brings remains to be assessed.

b. SST estimation

In section 4b above, we discussed the characteristics of SST retrieval using the 3.9 and 11 μm channels. The question arises as to whether the 13 μm channel, not traditionally used for SST, has any useful information content for SST estimation. The 13 μm channel is sensitive to the temperature of tropospheric carbon dioxide, as, to a smaller degree, is the 3.9 μm channel. This differential sensitivity to, in effect, air-sea temperature difference and lapse rate implies some potential for the former channel to add useful information about an aspect of the atmospheric correction in the latter channel. This is borne out in simulations of SST retrieval error using the three-channel combination 3.9, 11 and 13 μm , as shown in Figure 8. The retrieval accuracy is particularly improved in the cold, low-water vapor regime, where the 3.9 / 11 μm algorithm displays most scatter, for reasons already outlined in §3b. The overall simulated retrieval error is reduced from 0.36 K to 0.23 K by adding the 13 μm channel. For pre-operational validation of this new form of retrieval, see the companion paper by Harris et al. In brief, it appears that, in validation, the scatter of estimated SST is reduced by introducing the 13 μm channel. However, a large bias is present, and it appears that significant radiance bias correction (relative to our forward modeling configuration) of the 13 μm channel will be required before operational exploitation can occur. (As an aside, we can comment that, in simulation studies, using a 13 μm channel for SST in addition to the usual suite of SST channels at 3.9, 11 and 12 μm is found to reduce retrieval standard deviation by about 10%.)

6 Summary validation results and conclusions

A detailed analysis of the performance of the retrieval methods described above is provided by the companion paper of Harris et al. That paper extensively explores the relationships between biases in the SST retrievals and factors such as atmospheric state, zenith angle, Bayesian probability of cloudiness, and so on, and describes in detail the characteristics of the match-up database used. Here, we present some summary validation results that are consistent with those analyses, presenting results for both GOES-10 and GOES-12, in order to elucidate the effects of the absence of the 12 μm channel in the latter case.

Figure 9 shows distributions of GOES-10 SST minus matched drifting buoy SSTs. The results are separated into night and day cases. Recall that for GOES-10, night-time retrievals use three channels (3.9, 11 and 12 μm) and day-time retrievals use the split window channels (11 and 12 μm). The standard deviation (SD) of the distribution in Figure 9(a) is 0.58 K, which is less than the comparable value for day-time SSTs (0.84 K), partly because of the extra information added by the 3.9 μm channel. For both day and night cases there is a trend towards warm bias at low atmospheric correction (Figures 9(b) and 9(d)), i.e., at small values of the difference between the surface temperature and the 11 μm BT. This arises because of bias between the radiative transfer model (RTM) used to define coefficients and reality. Such bias can arise because of lack of realism of the atmospheric state assumed for the simulations, because of biases within the RTM, because of error in the instrumental characterization provided to the RTM, or because of other instrument calibration biases. Each of these can manifest as a trend relative to atmospheric correction because the effect of each bias source can be related to either atmospheric water vapour or scene brightness temperature, both of which correlate with atmospheric correction. Harris et al. look at these possibilities in detail, and deduce that instrument calibration and characterization errors are dominant, and require radiance bias correction.

The corresponding results for GOES-12 are shown in Figure 10. The night-time bias is -0.53 K and the night-time SD is 0.66 K (Figure 10(a)). This SD is greater than the GOES-10 equivalent, reflecting at least in part the lack of information from a 12 μm channel in the GOES-12 SST based on 3.9 and 11 μm . To assess the intrinsic potential of GOES-12 SST based on 3.9 and 11 μm , the coefficients were applied to an independent match-up database of night-time matches from the Ocean and Sea Ice Satellite Application facility (<http://www.osi-saf.org>). Using the most conservative cloud masking category for this MDB (confidence level 5), the bias is -0.27 K and the SD is 0.40 K. This SD is a significant improvement on the results in Figure 10 and is more representative of the quality of the coefficients under conditions of clear-skies as determined by a stricter cloud mask.

Despite using the same retrieval coefficients, the day-time GOES-12 SST has a broader SD of 0.89 K. This is partly the impact of having to use the pseudo-night-time 3.9 μm BT (although there is also greater variability between SST measured at buoy depth and the skin SST during the day, because of diurnal warming). The increased error in day-time GOES-12 SSTs is reflected in the products' SST error estimates, as described above. The trend with atmospheric correction for night-time data (Figure 10(b)) is similar to that for GOES-10, whereas there is little trend for the day time retrievals, Figure 10(d). This latter outcome must be somewhat fortuitous, since the retrieval equation is identical: a systematic effect in the correction of solar contamination happens to offset the trend that would otherwise be similar to that for night-time. There is a scattering of individual retrievals with errors exceeding +3 K, attributable to cases where the correction of solar contamination has proved inadequate. While "cold scatter", usually due to residual cloud contamination or excessive aerosol burden, is not uncommon in validation studies for single-view sensors, such "warm scatter" is a peculiarity of the GOES-12 daytime. In the latter case, the atmospheric contaminant may serve to increase the scattered solar component of the 3.9 micron channel which carries the highest weight in the retrieval (see value of a_3 coefficient of equation 4 in §3b).

GOES SST operations continue to develop with the aim of delivering improved products to users. There is therefore some difficulty in reporting in the scientific literature the techniques used, in that those techniques are evolving. Appropriately for an operational agency whose priority is security of product supply to users, there is also a lag between devising improved techniques and implementing them operationally to allow testing. In this article, we have therefore attempted to describe the key innovative elements of GOES-12 SST as operationally produced at time of writing, while fully acknowledging the limitations and approximations of the current approaches, and indicating the directions that will be taken in future operational upgrades.

The main advance described herein is the development of an operational methodology for the production of SST from GOES-12 Imager data. This in turn has necessitated the development of algorithms for the retrieval of SST in the daytime using the 3.9 and 11 μm channels. Since the former channel is subject to contamination from scattered and reflected solar radiation, algorithms have been devised to correct for these error sources that are fast enough to serve in the operational context. Further changes have included the revision of the nighttime SST retrieval to function without the 12 μm channel, and the adoption of a probabilistic physically-based cloud screening procedure. It should be noted that the new cloud detection scheme is applied to data from both operational GOES platforms. While it is recognized that the methodologies (particularly the correction for scattered solar radiation) are likely to require some enhancement, the validation results indicate that the SST product from GOES-12 achieves useful accuracy, even in day-time. Nonetheless, the results are inevitably degraded compared to the GOES-10 sensor. Finally, the product now includes the actual probability-of-clear-sky estimates for each pixel, although a traditional masked version (currently thresholded at $P_{\text{clear}} = 0.98$) is also available to maintain continuity. This may be regarded as a first step in the development of added value operational products for end-users which contain individual quantitative estimates of data accuracy for each pixel.

7. Acknowledgements

We thank Gerald Dittberner, Office of Systems Development, Mark De Maria, GIMPAP and Donald Gray, GOES-PSDI for providing the funding for this project. O Embury, C P Old and S N MacCallum were funded by NOAA/NESDIS. A. Harris and J Mittaz are funded through the NOAA Cooperative Institute for Climate Studies. Special thanks to the NESDIS Office of Satellite Data Processing for their work in operationalizing this GOES-12 SST product. The contents of this paper are solely the opinions of the authors and do not constitute a statement of policy, decision or position on behalf of NOAA or the US government. We thank the anonymous reviewers for helping us improve this manuscript, and in particular the reviewer who applied GOES-12 coefficients within the OSI-SAF MDB to generate a further point of comparison for the summary validation.

REFERENCES

- Brisson, A., Le Borgne, P., & Marsouin, A., 2002: Results of one year of preoperational production of sea surface temperatures from GOES-8, *J. Atmospheric & Oceanic Technology*, **19** (10), 1638-1652.
- Cox, C., and W. Munk, 1954: Measurement of the Roughness of the Sea Surface from Photographs of the Sun's Glitter. *J. Optical Society of America*, **44**, 838-850.
- Donlon C., I. Robinson, K. Casey, J. Vazquez, E. Armstrong, C. Gentemann, D. May, P. LeBorgne, J. Piolle, I. Barton, H. Beggs, D. J. S. Poulter, C. J. Merchant, A. Bingham, S. Heinz, A. Harris, G. Wick, B. Emery, A. Stuart-Menteth, P. Minnett, B. Evans, D. Llewellyn-Jones, C. Mutlow, R. Reynolds, H. Kawamura and N. Rayner, 2007: The Global Ocean Data Assimilation Experiment (GODAE) High Resolution Sea Surface Temperature Pilot Project (GHRSSST-PP), *Bull. Am. Met. Soc.*, **88** (8), 1197-1213. DOI: 10.1175/BAMS-88-8-1197
- Hale, G. M., and M.R. Querry, 1973: Optical constants of water in the 200-nm to 200mm. *Appl. Opt.*, **12**, 555-562.
- Harris A.R., C.J. Merchant, E.M. Maturi, O. Embury, S.N. MacCallum, W. Meng, J. Mittaz, C. Old, B. Potash, Validation of the NOAA operational geostationary sea surface temperature product from GOES-10 and GOES-12, *J. Atmos. Oceanic. Technol.*, submitted, 2007.
- Kidder, S.Q., and T.H. Vonder Haar, 1995: Satellite meteorology: an introduction. San Diego, Calif.; London: Academic Press, 466p.
- May, D. A. and W. O. Osterman, 1998: [Satellite-derived sea surface temperatures: Evaluation of GOES-8 and GOES-9 multispectral imager retrieval accuracy](#), *J. Atmos. Oceanic Technol.*, **15** (3), 788-797.
- Merchant, C. J., A. R. Harris, M. J. Murray and A. M. Zavody, 1999: Toward the elimination of bias in satellite retrievals of skin sea surface temperature 1. Theory, modeling and inter-algorithm comparison, *J Geophys Res*, **104**, C10, 23565-23578.
- Merchant, C. J., and P. Le Borgne, 2004: Retrieval of sea surface temperature from space based on modeling of infrared radiative transfer: Capabilities and limitations. *J Atmos. Oceanic Technol.*, **22**, 1734-1746.
- Merchant, C.J., A.R. Harris, E. Maturi, and S. MacCallum, 2005: Probabilistic physically based cloud screening of satellite infrared imagery of operational sea surface temperature retrieval. *Quart. J. Roy. Meteor. Soc.*, **131**, 2735-2755.
- Merchant, C. J., L.A. Horrocks, J. Eyre, and A.G. O'Carroll, 2006: Retrievals of sea surface temperature from infra-red imagery: origin and form of systematic errors. *Quart. J. Roy. Meteor. Soc.*, **132**, 1205-1223.
- Mackie, S., C. P. Old, O. Embury, C. J. Merchant, and P.N. Francis, 2008: Generalised Bayesian cloud detection for thermal satellite imagery. Part 1: Technique and validation over land and sea, *Int. J. Remote Sensing*, submitted.

Figure captions

Figure 1. Spectral responses and atmospheric spectral transmission. Dotted line: transmission for the standard MIPAS mid-latitude atmosphere (http://www-atm.physics.ox.ac.uk/RFM/rfm_downloads.html). Solid line: normalized spectral response functions for GOES-12 channels. Dashed line: normalized spectral response functions for ATSR-2 channels.

Figure 2. Contours of probability density in K^{-2} of local standard deviation of GOES-12 brightness temperatures (BTs) across a 3-by-3 pixel box, assuming radiometric noise of 0.15 K at 3.9 μm , 0.20 K at 11 μm , and a 10% probability of a front of strength 0.15 $K km^{-1}$.

Figure 3. Joint probability density functions for (left panel) brightness temperature and (right panel) local standard deviation (LSD) used to represent cloudy observations of the GOES-12 imager. Lines are contours of (left panel) $10^6 \times$ probability per K^2 of observing a given pair of brightness temperatures, and (right panel) probability per K^2 of observing a given pair of LSDs.

Figure 4. Simulations of error in GOES-12 3.9/11 μm sea surface temperature retrievals plotted against sea surface temperature. Diamonds: satellite zenith angles below 40°; triangles: zenith angles between 40° and 60°; squares: zenith angles between 60° and 70°.

Figure 5. Geometry of simulations for radiative transfer modeling for defining GOES-12 retrieval coefficients. Numerical weather prediction profiles are obtained according to the sampling strategy of Merchant et al. (1999) (squares), with some additional sampling in key areas (diamonds).

Figure 6. Parameterization of effect of path-scattered radiance on the 3.9 μm channel brightness temperature. (a) Upper panel: Scatter plot of parameterized estimates (“Predicted ΔT_b ”) against effect fully simulated by MODTRAN4 (“Modtran ΔT_b ”), for surface meteorological visibility of 23 km. Darker squares indicate a greater density of points within the square. (b) Right panel: As (a) but with a fixed 27 km visibility assumed for the predicted values, against MODTRAN4-simulated values for visibilities of 50 km (distribution with dotted contour lines) and 23 km (distribution with solid contour lines).

Figure 7: Brightness temperature at 3.9 μm minus that at 11 μm for two extracts from GOES-12 imagery, dates and times as indicated. Areas of large positive difference are associated with elevated brightness temperature in the 3.9 μm channel from sun-glint (near-circular areas) and/or reflection from clouds (mottled features). Black areas are land-masked areas of central and south America; grey areas are off-scale (difference exceeding 20 K). Overlaid are contours of estimated change in 3.9 μm brightness temperature due to glint.

Figure 8. As fig 4, but for SST retrieval using 3.9, 11 and 13 μm channels together.

Figure 9. Summary validation results for the GOES-10 sensor. (a) Frequency distribution of retrieved minus drifting buoy SST, night-time cases. (b) Distribution of difference of retrieved SST from drifting buoy SST against atmospheric correction at 11 μm . Density of shading reflects the relative population density of points, with >99% of points being in mid-grey to black areas. (c) and (d) As (a) and (b) but for day-time cases.

Figure 10. As Figure 9, for GOES-12 SSTs.

Figures

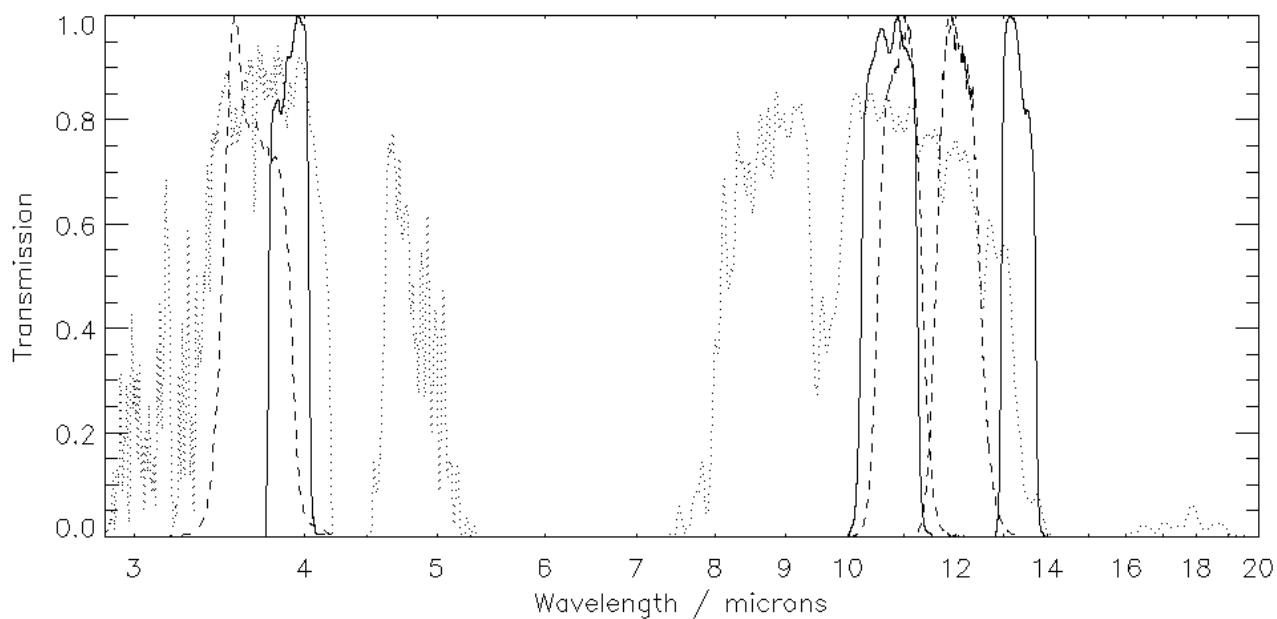


Figure 1. Spectral responses and atmospheric spectral transmission. Dotted line: transmission for the standard MIPAS mid-latitude atmosphere (http://www-atm.physics.ox.ac.uk/RFM/rfm_downloads.html). Solid line: normalized spectral response functions for GOES-12 channels. Dashed line: normalized spectral response functions for ATSR-2 channels.

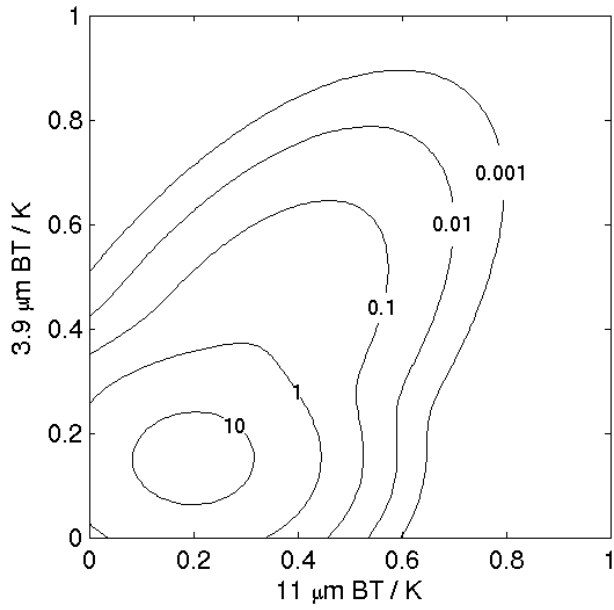


Figure 2. Contours of probability density in K^{-2} of local standard deviation of GOES-12 clear-sky brightness temperatures (BTs) across a 3-by-3 pixel box, assuming radiometric noise of 0.15 K at 3.9 μm , 0.20 K at 11 μm , and a 10% probability of a front of strength 0.15 K km^{-1} .

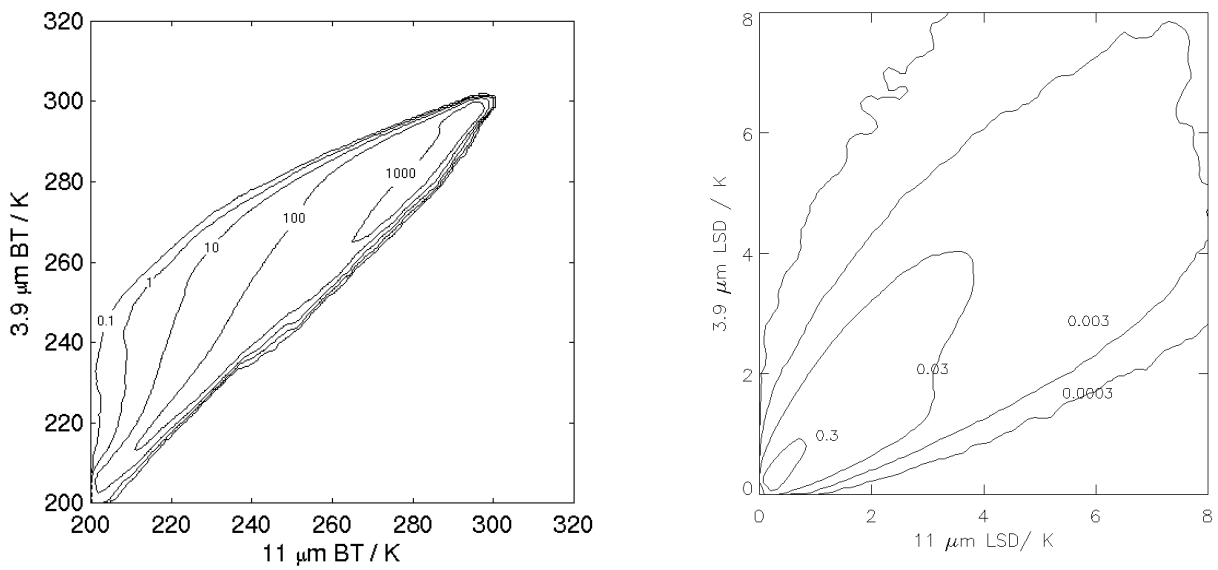


Figure 3. Joint probability density functions for (left panel) brightness temperature and (right panel) local standard deviation (LSD) used to represent cloudy observations of the GOES-12 imager. Lines are contours of (left panel) $10^6 \times$ probability per K^2 of observing a given pair of brightness temperatures, and (right panel) probability per K^2 of observing a given pair of LSDs.

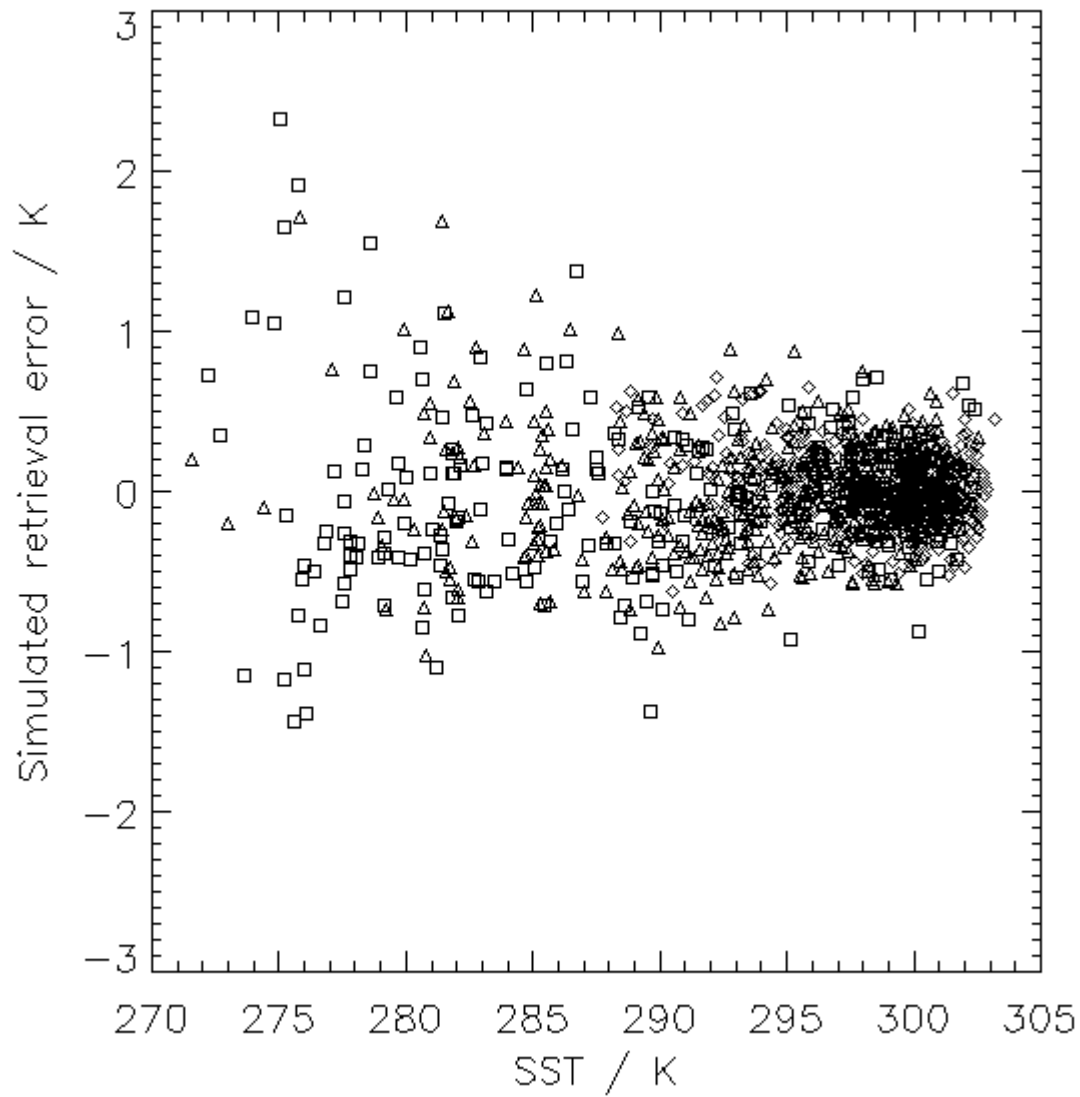


Figure 4. Simulations of error in GOES-12 3.9/11 μm sea surface temperature retrievals plotted against sea surface temperature. Diamonds: satellite zenith angles below 40° ; triangles: zenith angles between 40° and 60° ; squares: zenith angles between 60° and 70° .

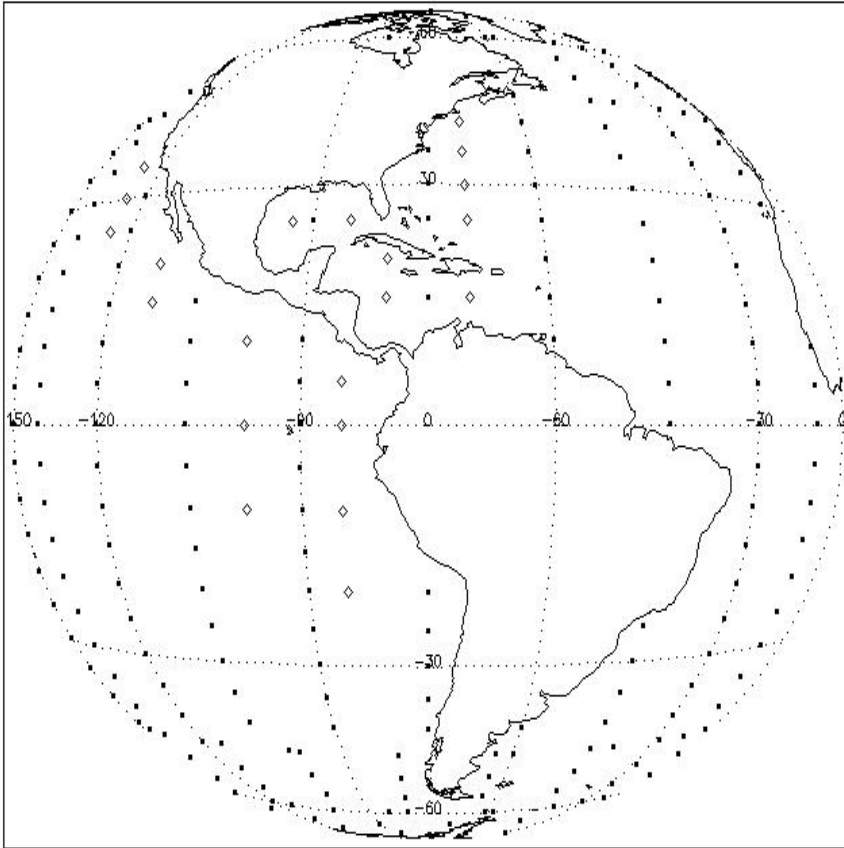


Figure 5. Geometry of simulations for radiative transfer modeling for defining GOES-12 retrieval coefficients. Numerical weather prediction profiles are obtained according to the sampling strategy of Merchant et al. (1999), squares, with some additional sampling in key areas (diamonds).

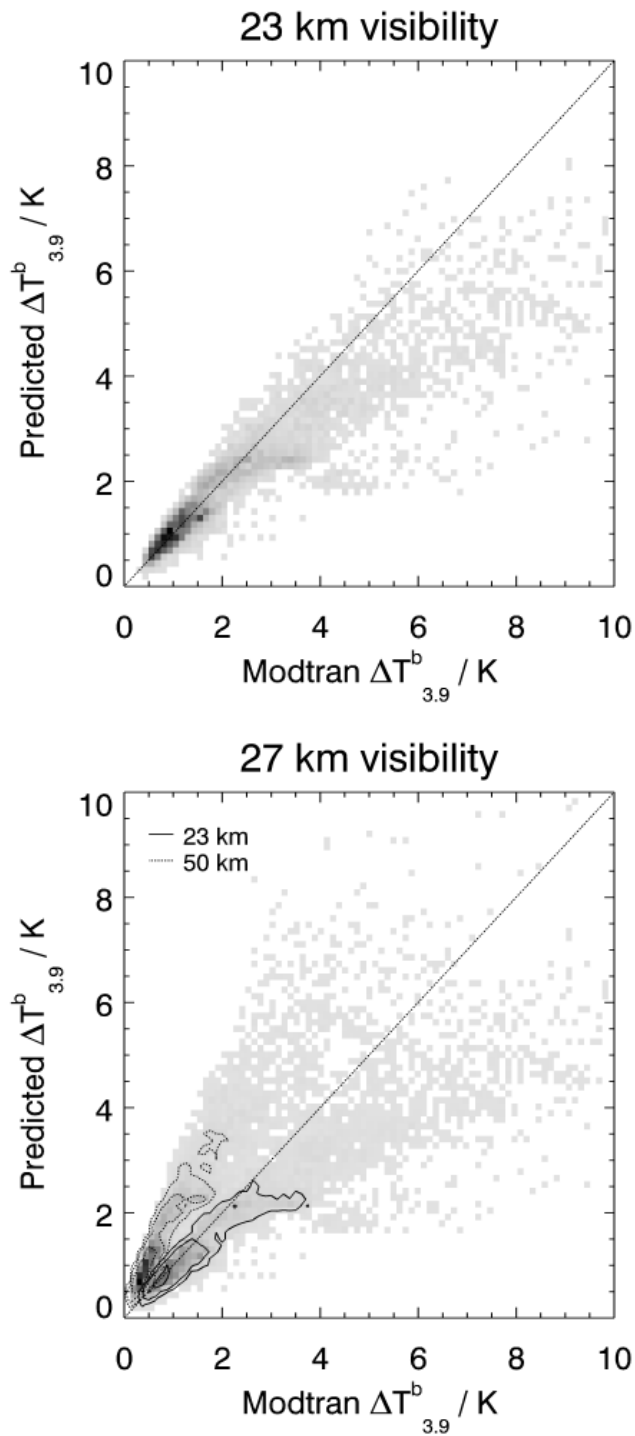


Figure 6. Parameterization of effect of path-scattered radiance on the 3.9 μm channel brightness temperature. (a) Upper panel: Scatter plot of parameterized estimates (“Predicted ΔT_b ”) against effect fully simulated by MODTRAN4 (“Modtran ΔT_b ”), for surface meteorological visibility of 23 km. Darker squares indicate a greater density of points within the square. (b) Lower panel: As (a) but with a fixed 27 km visibility assumed for the predicted values, against MODTRAN4-simulated values for visibilities of 50 km (distribution with dotted contour lines) and 23 km (distribution with solid contour lines).

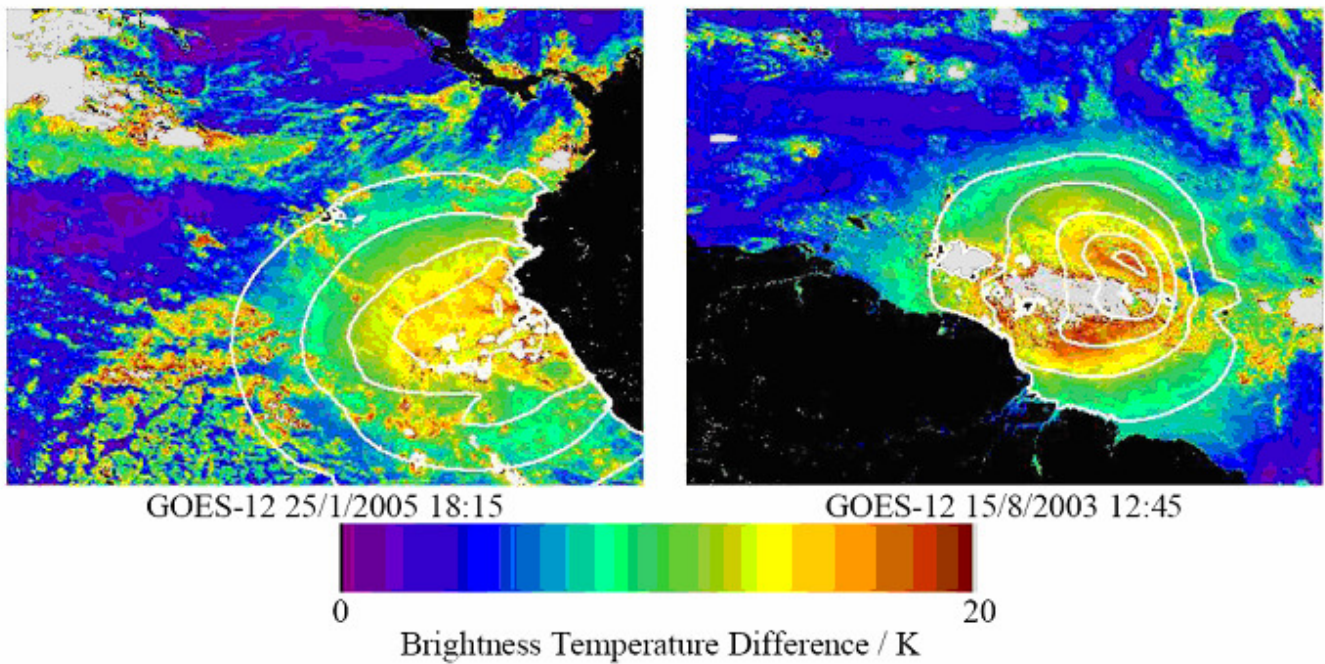


Figure 7: Brightness temperature at $3.9 \mu\text{m}$ minus that at $11 \mu\text{m}$ for two extracts from GOES-12 imagery, dates and times as indicated. Areas of large positive difference are associated with elevated brightness temperature in the $3.9 \mu\text{m}$ channel from sun-glnt (near-circular areas) and/or reflection from clouds (mottled features). Black areas are land-masked areas of central and south America; grey areas are off-scale (difference exceeding 20 K). Overlaid are contours of estimated change in $3.9 \mu\text{m}$ brightness temperature due to glint, the outer contour being that for 1 K.

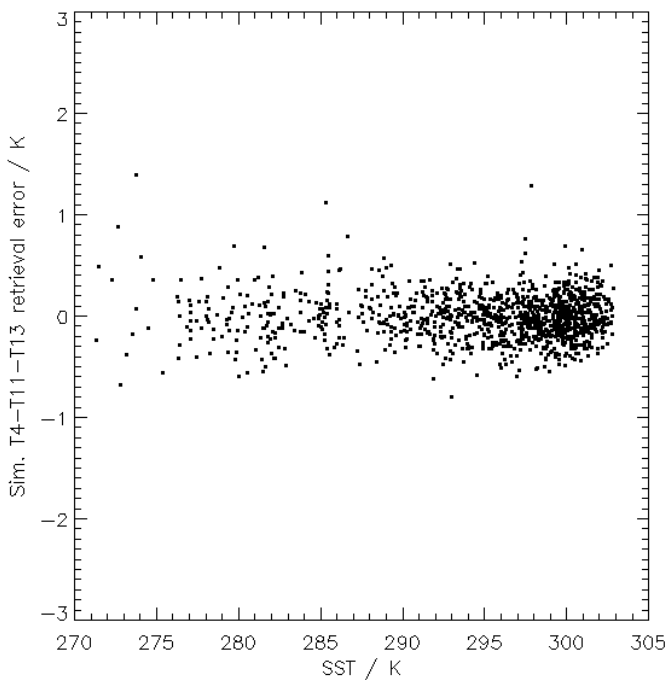


Figure 8. As fig 4, but for SST retrieval using 3.9 , 11 and $13 \mu\text{m}$ channels together.

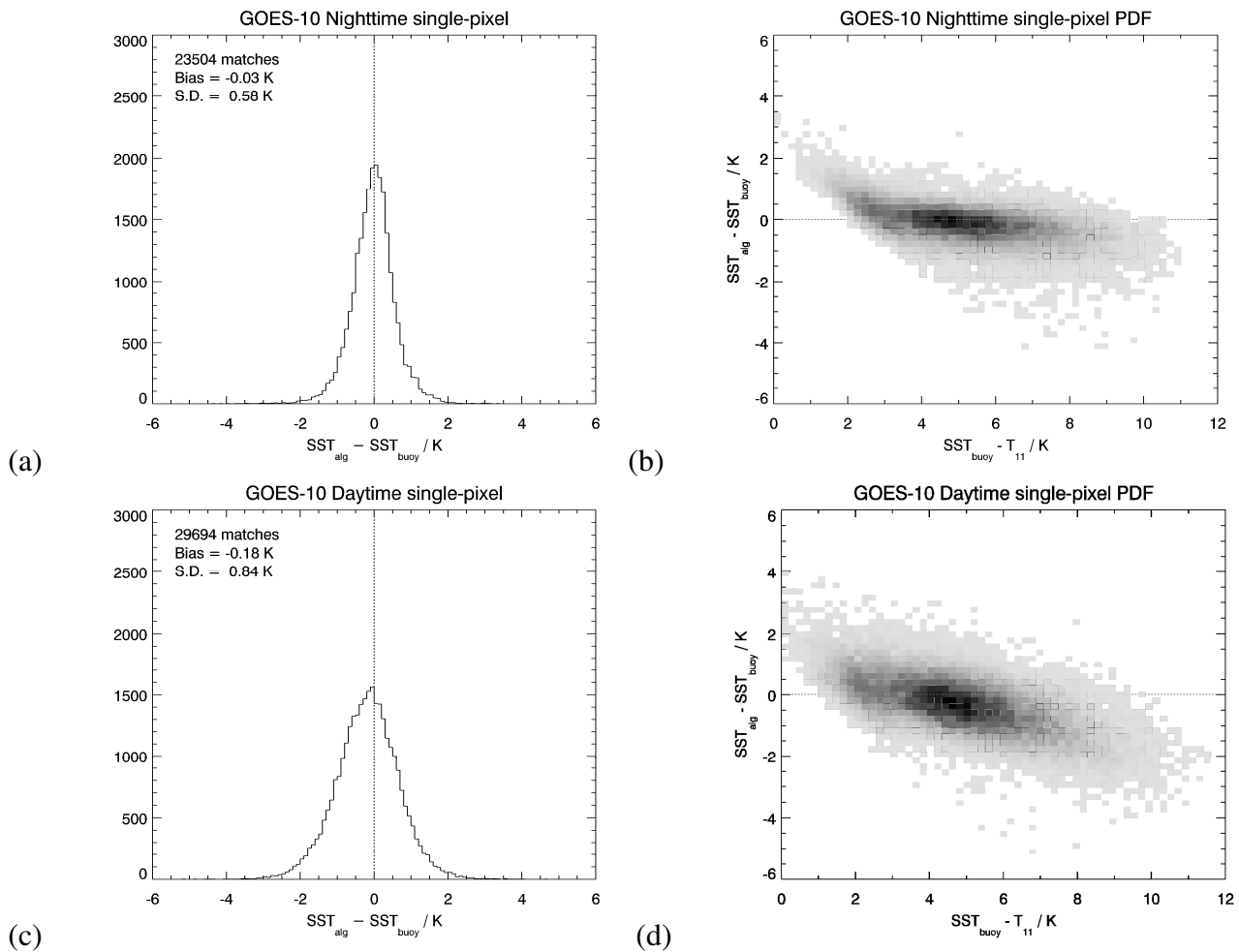
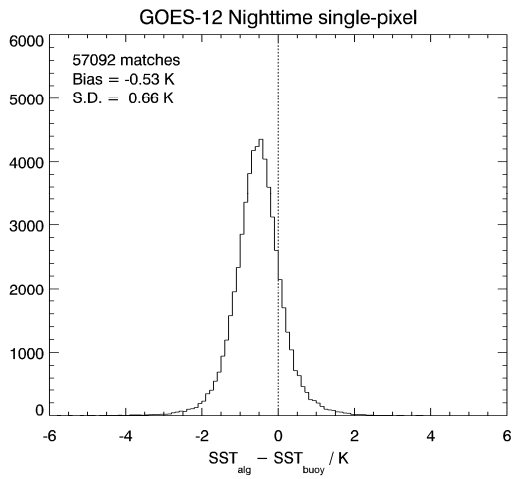
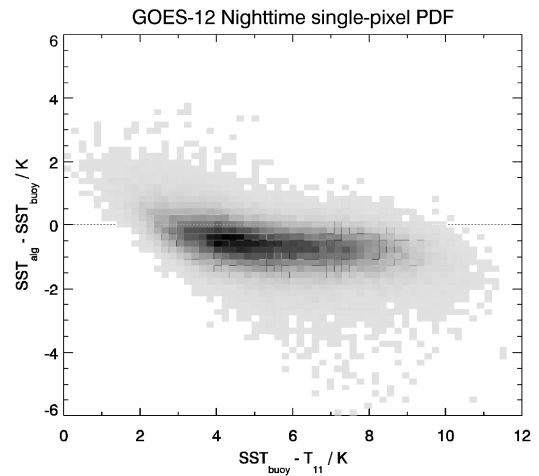


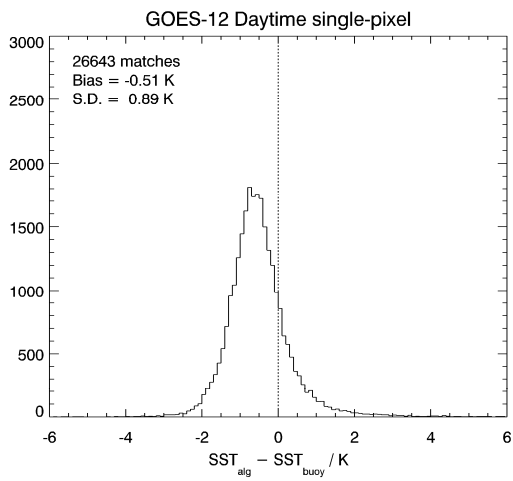
Figure 9. Summary validation results for the GOES-10 sensor. (a) Frequency distribution of retrieved minus drifting buoy SST, night-time cases. (b) Distribution of difference of retrieved SST from drifting buoy SST against atmospheric correction at 11 μm . Density of shading reflects the relative population density of points, with >99% of points being in mid-grey to black areas. (c) and (d) As (a) and (b) but for day-time cases.



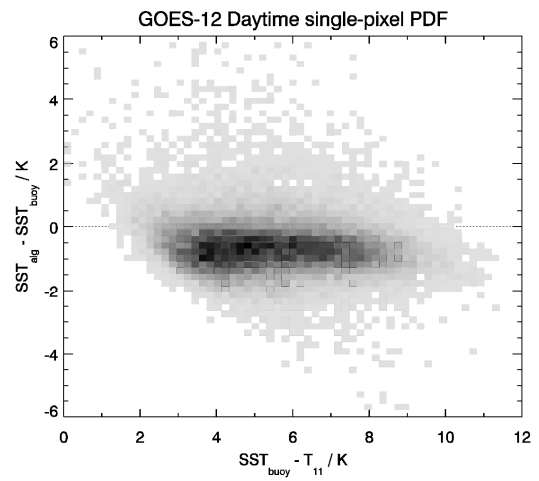
(a)



(b)



(c)



(d)

Figure 10. As Figure 9, for GOES-12 SSTs.